Nuclear Science and Techniques (2026) 37:25
https://doi.org/10.1007/s41365-025-01830-0

HALIMA: a hybrid array for lifetime measurement of neutron-rich nuclei at IMP

Zi-Hao Jia[1,2] · Yong-De Fang[1,2] · Si-Cheng Wang[1,2] · Wei Hua[3,4] · Hong-Yi Wu[5,6] · Guang-Xin Zhang[3] · Cen-Xi Yuan[3] · Zhi-Xuan Wang[3] · Jun-Hong Xu[1,2] · Jian-Hong Li[1,2] · Wen Liang[1,2] · Yu-Hong Tan[1,2] · Wen-Jun Pan[6] · Yu-Xuan Ren[6] · M. Kumar Raju[7] · Song Guo[1,2] · Guang-Shun Li[1,2] · Yun-Hua Qiang[1,2] · Min-Liang Liu[1,2] · Bing Ding[1,2] · Ming-Hui Huang[1,2] · Ning-Tao Zhang[1,2] · Bing-Shui Gao[1,2] · Peng Ma[1,2] · He-Run Yang[1,2] · Ruo-Fu Chen[1,2] · Hai-Xia Li[1,2] · Rong-Hua Li[1,2] · Xiu-Hua Wang[1,2] · Cui-Hong Chen[1,2] · Hai-Bo Yang[1,2] · Jian-Song Wang[8] · Xiao-Hui Sun[8] · Zhi-Huan Li[6] · Hui Hua[6] · Wei Wang[3] · Xin-Xing Xu[1,2] · Xiao-Hong Zhou[1,2] · Zai-Guo Gan[1,2] · Yu-Hu Zhang[1,2]

Received: 30 June 2025 / Revised: 14 August 2025 / Accepted: 23 August 2025 / Published online: 3 January 2026

Abstract

A new multi-detector array named HALIMA (Hybrid Array for LIfetime MeAsurement) has been developed at Lanzhou for nuclear structure studies in fission. The array comprises eight BGO-shielded High-Purity Germanium detectors and twenty fast Ce-doped Lanthanum Bromide [$LaBr_3$(Ce)] detectors shielded with CsI(Tl). HALIMA is further complemented by two ancillary detector systems: fission fragment (FF) detectors and β detectors. This configuration enables precise sub-nanosecond lifetime measurements using the fourfold FF/β-Ge-$LaBr_3$(Ce)-$LaBr_3$(Ce) coincidence technique. The performance and specifications of the detectors, associated electronics, and the data acquisition system are presented in detail. The advantage of FF selectivity is emphasized, which significantly enhances sensitivity to specific fission channels. Using this approach, the lifetimes of the nuclear excited states populated in the spontaneous fission of ^{252}Cf were measured, showing good agreement with the established literature values.

Keywords FFs/β-γ rays coincidences · Selectivity · Spontaneous fission · $LaBr_3$(Ce) · HPGe · Solar cells · Lifetime measurement

1 Introduction

Measurement of the lifetimes of nuclear excited states is a fundamental aspect of nuclear structure studies. These lifetimes are directly related to the reduced transition probabilities, which provide essential information about the underlying nuclear structure, including the degree of overlap between the initial and final nuclear wave functions. Precise lifetime data are crucial for testing nuclear models and understanding the collective and single-particle excitations across various regions of the nuclear chart. Over the past two decades, the development of the fast scintillator $LaBr_3$ (Ce) has opened the possibility of performing fast-timing measurements on the lifetimes of nuclear states ranging from nanoseconds to picoseconds [1]. Several dedicated fast-timing arrays have been developed since then, including FATIMA [2], KHALA [3], and VESPA [4]. When coupled

---

This work was supported by the National Natural Science Foundation of China (Nos. 12275321, 12121005, 12475129, and 12335009), the Natural Science Foundation of Guangdong Province, China (No. 2025A1515012112), the International Atomic Energy Agency Coordinated Research Project F41034 (No. 28649), the computational resources from Sun Yat-sen University the National Supercomputer Center in Guangzhou, the Open Project of Guangxi Key Laboratory of Nuclear Physics and Nuclear Technology (No. NLK2023-08), the Central Government Guidance Funds for Local Scientific and Technological Development, China (No. Guike ZY22096024), the Guangdong Major Project of Basic and Applied Basic Research (No. 2021B0301030006), Young Scientists Fund of the National Natural Science Foundation of China (No. 12405144), and the National Key Research and Development Program (MOST 2022YFA1602304).

Extended author information available on the last page of the article with a Ge array, these arrays are used in triple Ge-LaBr$_3$(Ce)-LaBr$_3$(Ce) coincidence measurements, allowing a wide range of excited-state lifetimes in neutron-rich nuclei to be studied. This method leverages the superior energy resolution of Ge detectors to isolate specific transitions of interest, whereas the coincident γ-γ events recorded by the LaBr$_3$(Ce) array were used to perform precise fast-timing analyses. More recently, extensive lifetime measurement studies have been performed using combined setups such as EXILL & FATIMA [5], ν-ball & FATIMA [6], and GAMMASPHERE & FATIMA [7] using thermal and fast neutron-induced fission, as well as ^{252}Cf spontaneous fission source. However, achieving high selectivity and effective background suppression is a major challenge in such studies. In any fission process, hundreds of different fission fragments are produced, with each fragment typically emitting approximately seven γ-rays. The accurate association of these γ-rays with their corresponding fission products with an intense background is experimentally demanding. To obtain clean data, it is essential to enhance selectivity and minimize background contributions.

To overcome the limitations associated with using a Ge array alone, various fission-tagging devices have been developed to enhance the selectivity. One notable example is the integration of a liquid scintillator-based active fission target into the FIPPS spectrometer at the ILL [8]. This active target enables the identification of fission fragments and their temporal correlation with the subsequent γ decay, allowing efficient suppression of the uncorrelated γ-ray background originating from β decay. To further improve the selectivity and suppress the background originating from nonspecific fission products, mass-identified fission fragment FIFI spectrometers with a resolution of approximately six mass units have been employed in isomer decay spectroscopy studies [9].

To enhance the selectivity and suppress the background, a dedicated hybrid setup HALIMA (Hybrid Array for Lifetime MeAsurement, HALIMA) was developed at the Institute of Modern Physics, Chinese Academy of Sciences, China. HALIMA is specifically designed to measure the sub-nanosecond lifetimes of neutron-rich nuclei produced via fission. The array consists of eight Compton-suppressed HPGe and twenty LaBr$_3$(Ce) detectors with CsI(Tl)-based anti-Compton shields for γ-ray detection. In addition, two auxiliary detector arrays, 36 solar cell detectors, and 36 fast plastic scintillators were integrated into the HALIMA setup to detect fission fragments and β particles. With fragment tagging via solar cells and β-particle tagging via plastic scintillators, HALIMA enables the simultaneous application of both FF-Ge-LaBr$_3$(Ce)-LaBr$_3$(Ce) and β-Ge-LaBr$_3$(Ce)-LaBr$_3$(Ce) fast-timing techniques. A key component of the HALIMA setup is the solar cell array, which registers the implantation of fission fragments and correlates them spatially and temporally with their subsequent γ decay, thereby effectively serving as a fission tag. As demonstrated later, the application of mass-identified fission tagging reduces the background from other fragments by more than a factor of four. In addition to fission tagging, the use of CsI(Tl)-shielded LaBr$_3$(Ce) detectors in Compton suppression mode enhances the peak-to-total ratio by a factor of 1.5. To further optimize the detection, the LaBr$_3$(Ce) array in HALIMA was designed to have twice the efficiency of the Ge array, thereby maximizing the overall Ge-LaBr$_3$(Ce)-LaBr$_3$(Ce) coincidence efficiency.

In this paper, a comprehensive description of the HALIMA detection system is presented, including its detector components, readout electronics, and fully digital data acquisition system. The results of the first experiment using a ^{252}Cf spontaneous fission source are discussed to illustrate the performance of the setup. Section 2 details the detector hardware and data acquisition system. Section 3 describes the data analysis techniques employed for fast-timing measurements across different time ranges. A summary and outlook are provided in Sect. 4.

2 Instruments

An overview of the HALIMA detection system is shown in Fig. 1, which illustrates the arrangement of the HPGe and LaBr$_3$(Ce) detectors, along with the data acquisition setup. The following sections describe the configuration and integration of each component in detail.

2.1 HPGe detectors

The HALIMA setup includes eight n-type coaxial HPGe detectors, each equipped with BGO shielding, mounted on the central ring perpendicular to the fission axis. The crystals of the HPGe detectors are 71 mm in diameter and 72 mm long. The distance between the entrance window of the HPGe detectors and the center of the array is 17.5 cm. Each detector offers a relative efficiency of 70% compared to a standard 3 inches × 3 inches NaI(Tl) detector, with a typical energy resolution of 2.5 keV (FWHM) at 1332 keV. The full-energy peak (FEP) efficiency at 1 MeV was measured as 1.05% using standard ^{152}Eu, ^{133}Ba, and ^{60}Co radioactive sources. The resulting absolute efficiency curves are presented in Fig. 2, along with a fit using the empirical formula described in Ref. [10].

Each HPGe detector in the HALIMA setup is surrounded by a BGO anti-Compton shield composed of eight optically isolated BGO crystals, each coupled to a photomultiplier tube (PMT). For each BGO anti-Compton shield, the PMTs are daisy-chained to obtain a single summed output signal. These BGO Compton suppressors significantly reduce the

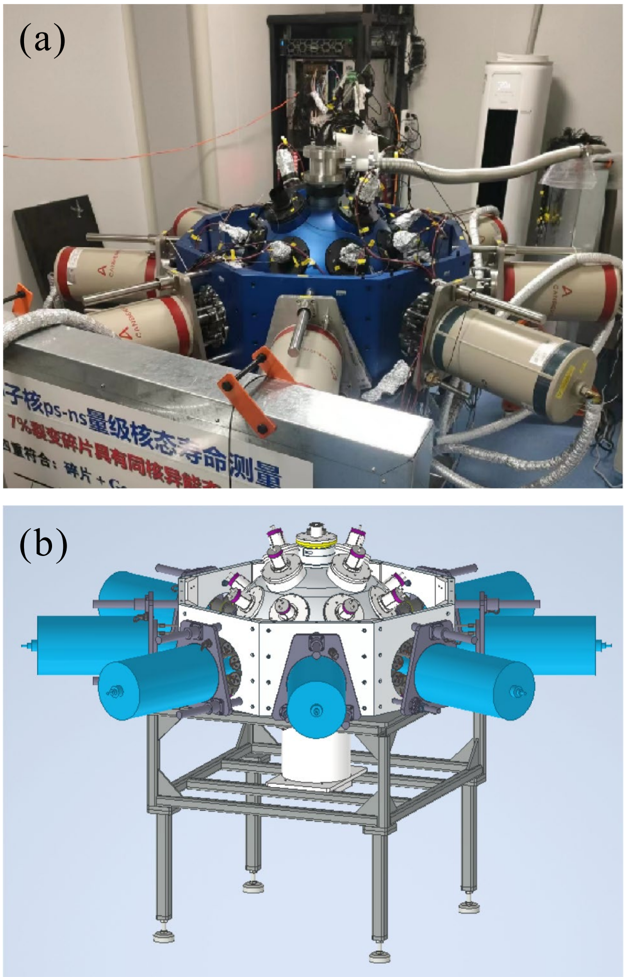

Fig. 1 (Color online)**a** Photograph of the HALIMA setup at the Institute of Modern Physics (IMP). Eight HPGe detectors are mounted on the central ring in a horizontal configuration. Two of the three rings of the $LaBr_3$(Ce) detectors are also visible. The digital data acquisition system and high-voltage supply are located behind the array. **b** Technical schematic of the complete HALIMA setup

background, providing a suppression of approximately 77% in the 400–800 keV energy range when tested with a ^{60}Co source.

2.2 $LaBr_3$(Ce) detectors

To facilitate the lifetime measurements, 20 individual $LaBr_3$(Ce) detectors were incorporated into the HALIMA setup, all configured identically. Each detector consists of a cylindrical $LaBr_3$(Ce) crystal with a diameter of 2 inches and length of 3 inches, coupled to a Hamamatsu R13089 photomultiplier tube. As shown in Fig. 1, two rings consisting of eight $LaBr_3$(Ce) detectors each have been mounted on both sides of the central ring of HPGe detectors, positioned at angles of 56° and 124° relative to the fission axis. The distance from the detector face to the center of the array is 16.5 cm. Additionally, a third ring composed of four $LaBr_3$(Ce) detectors is mounted on the topmost layer of the array, with each detector located 22 cm from the center and oriented at an angle of 29° with respect to the fission axis. This configuration provides a solid-angle coverage of approximately 13% for an isotropic source located at the center of the array.

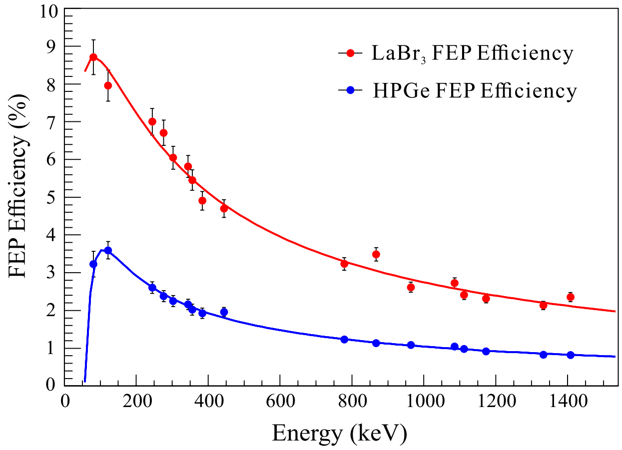

Fig. 2 (Color online)The absolute full-energy peak efficiency as a function of γ energy as measured using ^{152}Eu, ^{133}Ba, and ^{60}Co γ sources. The red circle represents the FEP of $LaBr_3$(Ce) detectors fitted in red line, while the FEP of HPGe detectors is shown in blue circle fitted in blue line

Owing to the compact size of $LaBr_3$(Ce) crystals, Compton scattering is significant, resulting in a pronounced Compton continuum that reduces the peak-to-total ratio, particularly for low-energy γ-rays [11]. To reduce Compton continuums, Régis [12] and Gierlik [13] et al. developed a BGO-based Compton suppressor for a $LaBr_3$(Ce) detector and achieved significant improvements in the peak-to-total ratio [12] and peak-to-Compton ratios [13]. In the present work, a more cost-effective, compact, and novel CsI(Tl)-based anti-Compton shield was developed and installed in the HALIMA setup. Figure 3 shows a technical drawing of a single $LaBr_3$(Ce) detector housed within a CsI(Tl) anti-Compton shield supported by an aluminum shell. Each $LaBr_3$(Ce) detector is enclosed by a CsI(Tl) anti-Compton shield composed of four separated CsI(Tl) crystals. The scintillation signals from these crystals are read out using twenty-eight 6.4 mm × 6.4 mm silicon photomultipliers (SiPMs), with seven SiPMs coupled to each crystal. These signals were summed and read out as a single channel. A comparative study using a calibrated ^{152}Eu source (Fig. 4) demonstrates that the intense Compton background is significantly reduced when the CsI(Tl) anti-Compton shield is applied. A more detailed characterization and performance analysis will be presented in a forthcoming publication.

To optimize the time resolution of $LaBr_3$(Ce) detectors in γ-γ coincidence mode, the PMTs of the $LaBr_3$(Ce) detectors

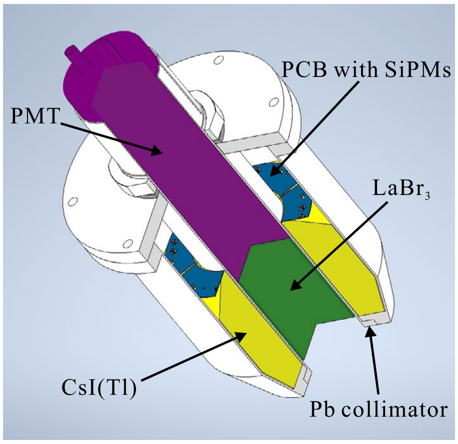

Fig. 3 (Color online)The technical drawing of three-quarter section of a single module of $LaBr_3$(Ce) detector with CsI(Tl) anti-Compton shields encapsulated within an aluminum shell. The individual $LaBr_3$ (Ce) detector is composed of a $LaBr_3$(Ce) crystal (green) coupled to a PMT (purple) surrounded by four CsI(Tl) crystals (yellow). The SiPMs are employed as the readout for CsI(Tl) anti-Compton shields, which are mounted on PCB (blue)

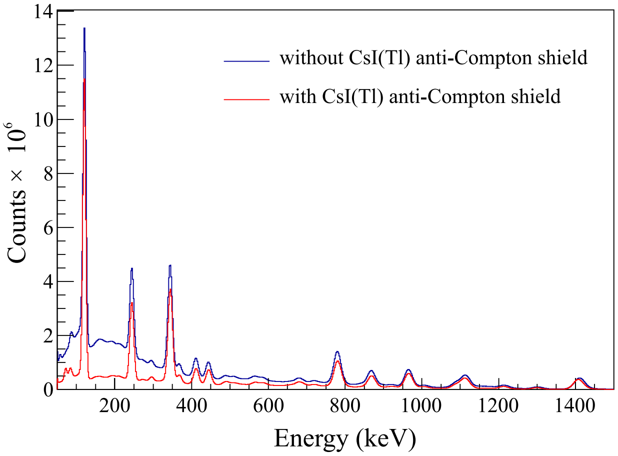

Fig. 4 (Color online)The energy projection spectra of the symmetric γ-γ coincidence matrix of $LaBr_3$(Ce) detectors obtained using ^{152}Eu standardized source. Compared to the spectrum without CsI(Tl) anti-Compton shields (blue), the background continuums are effectively reduced with the use of CsI(Tl) anti-Compton shields in the energy spectrum (red)

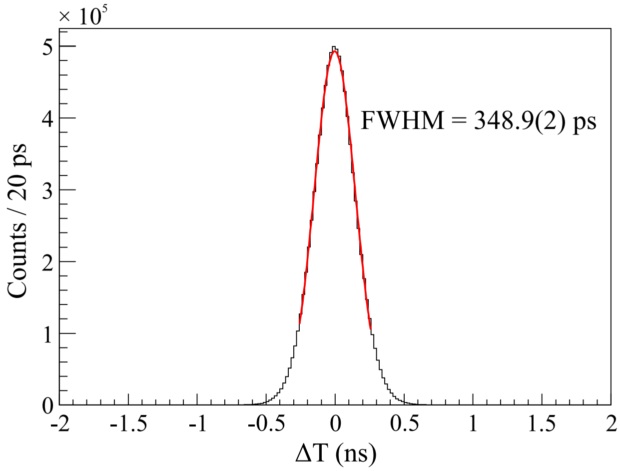

Fig. 5 Time distribution of twenty $LaBr_3$(Ce) detectors in HALIMA from the 1173–1332 keV γ-ray cascade of ^{60}Co source. Time resolution for twenty $LaBr_3$(Ce) detectors was fitted by Gaussian function

were operated at a bias voltage of approximately –1070 V. At this voltage, the 662 keV γ-rays from a ^{137}Cs source produced a uniform output signal amplitude of 200 mV across all detectors. Because the inherent nonlinearity in the energy response of $LaBr_3$(Ce) detectors is largely attributed to the voltage sensitivity of PMTs, a second-order polynomial function was employed for energy calibration. Standard γ -ray sources, ^{133}Ba and ^{152}Eu, were used for this calibration, covering an energy range of 81 keV to 1408 keV. The energy resolution of the $LaBr_3$(Ce) detectors was found to be 2.67% at the 1332 keV line of a ^{60}Co source. The absolute full-energy peak (FEP) efficiency at 1 MeV for the entire $LaBr_3$ (Ce) array was measured to be 2.74%. The corresponding absolute efficiency curves along with the fitting results are presented in Fig. 2.

The two primary timing characteristics of the $LaBr_3$ (Ce) detector array are the time resolution and time walk. The time resolution was determined from the summed time difference spectra of all pairwise combinations among the 20 $LaBr_3$(Ce) detectors. To achieve this, the individual time spectra were aligned by applying appropriate time shifts to each detector relative to a chosen reference detector, after which the summed time difference spectrum was obtained using ^{60}Co source. The time information was extracted using the TSINC digital algorithm [14] and Constant Fraction Discrimination (CFD). Figure 5 displays the resulting time difference distribution for 20 $LaBr_3$(Ce) detectors with 1173–1332 keV γ-rays of ^{60}Co source. The time resolution is 348.9(2) ps in FWHM, which is comparable to the resolution of FATIMA [2] despite the larger crystal volume of the $LaBr_3$(Ce) detectors used in our setup.

To extract lifetimes shorter than the intrinsic time resolution of $LaBr_3$(Ce) detectors to a few picoseconds (ps), it is essential to determine the Prompt Response Difference (PRD) as a function of energy. PRD calibration is used to describe the time walk characteristics using the coincident γ-ray cascade emitted by ^{152}Eu source over the energy range of 200–1400 keV. The PRD was measured using Leading-Edge Discrimination (LED) in conjunction with the TSINC interpolation algorithm [14]. The resulting PRD curve is presented in the top panel of Fig. 6 and was fitted using the following equation:

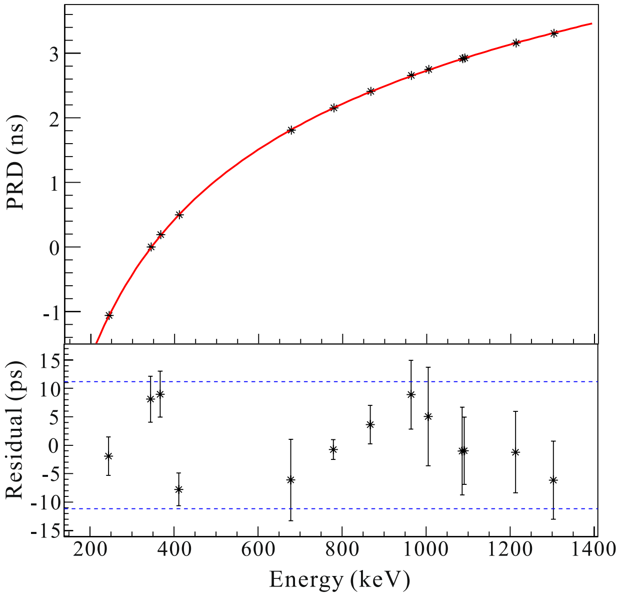

Fig. 6 The energy-dependent prompt response difference (PRD) curve for LaBr$_3$(Ce) detectors obtained using ^{152}Eu source for the reference energy of 344 keV shown in the top panel. The bottom panel shows the residuals of the PRD calibration function fit as described by Eq. (1) with twice the overall PRD calibration uncertainty of 11 ps

$$\mathrm{PRD}(E_\gamma) = \frac{a}{\sqrt{E_\gamma + b}} + cE_\gamma + d. \tag{1}$$

From the residuals shown in the lower panel of Fig. 6, the uncertainty in the PRD is estimated to be ± 5.5 ps. With PRD, the generalized centroid difference (GCD) method [15] can be applied for precise lifetime measurements down to tens of picoseconds (ps). A detailed account of PRD calibration and its application in this setup will be presented in a forthcoming publication.

2.3 FFs detectors: solar cells

The detection of fission fragments (FFs) in an intense background dominated by light charged particles remains a major challenge in fission experiments. Solar cells, originally developed for photovoltaic energy conversion, were first introduced by Siegert in 1979 for the detection of FFs at the Institut Laue-Langevin (ILL) facility [16]. Subsequently, Ajitanand et al. demonstrated their radiation hardness during a ^{252}Cf experiment, thereby confirming their suitability for use in high-background environments [17]. Owing to its low cost, flexible geometry, and insensitivity to alpha particle, solar cells have been effectively employed in fission detection arrays, such as SAPHIR [18, 19] and DEATH-STAR [20, 21].

In this study, the rise time and pulse-height characteristics of three commercially available solar cells were evaluated. Among them, TOPCON-type solar cells were selected as FF detectors because of their high signal amplitude (400–600 mV) and relatively fast rise time (200–800 ns). These solar cells have a thickness of ~ 130 μm and a very small depletion depth (~ 1 μm), making them largely insensitive to light charged particles, such as alpha particles, because of their charge collection mechanism, specifically the funneling mechanism [22]. As illustrated in Fig. 7, the solar cells array, consisting of thirty-six 11 mm × 11 mm solar cells, mounted on a printed circuit board (PCB) positioned at the center of HALIMA setup. The raw pulse-height spectrum of the FFs from a ^{252}Cf source detected by a solar cell is shown in Fig. 8. To assess the mass resolution of the TOPCON solar cells, the 2E method

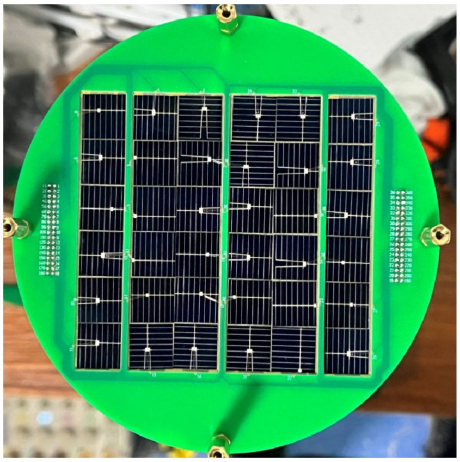

Fig. 7 (Color online)Solar cell array used as implantation detectors in the present work. A total of 36 solar cells, each measuring 11 mm × 11 mm, were mounted on a PCB and connected to the signal outputs. The assembled PCB is positioned at the center of the HALIMA setup

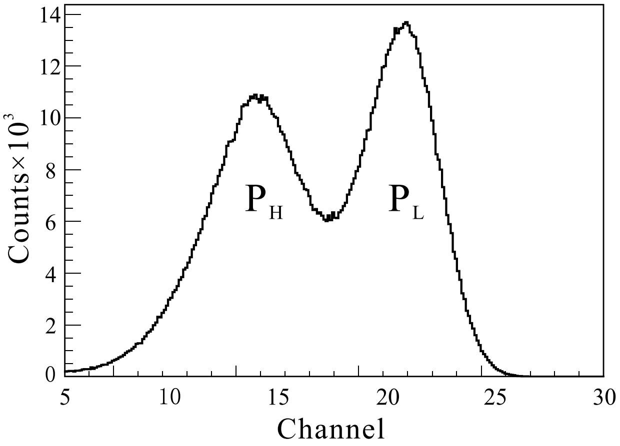

Fig. 8 The raw pulse-height spectrum of fission fragments of ^{252}Cf source detected by a solar cell. P_H and P_L represent the pulse height of heavy and light fragments, respectively

[23], which is based on the conservation laws of mass and momentum, was applied using an open ^{252}Cf source. Schmitt calibration [24] was used in this analysis, with the primary equation expressed as:

$$E = (a + a'M)x + b + b'M, \tag{2}$$

where a, a', b, and b' are constants using the values in Ref. [25], and E, x, and M represent the energy, pulse height, and mass of the FFs, respectively. Subsequently, an iterative process based on the neutron emission distribution [26] was performed to determine both the pre-neutron and post-neutron mass distributions. The resulting FF mass distribution is presented in Fig. 9 and compared with the data from Ref. [26], demonstrating good agreement. The typical time resolution of solar cells in the present work was approximately 20 ns, using a standard charge-sensitive preamplifier.

When solar cells are used as FF detectors in fission experiments, it is essential to evaluate their radiation damage tolerance. For this purpose, a comparative radiation damage test was performed using a 20 mm × 20 mm silicon detector and a solar cell of the same size. Both detectors were placed 8 cm from a ^{252}Cf source with an activity of 100 μCi (3.7 MBq). The variation in the pulse height as a function of the incident flux is shown in Fig. 10. For an integrated flux of approximately 10^9 particles/cm^2, the FFs detected by the solar cell exhibited only a 10–15% reduction in pulse height, indicating a minor degradation. In contrast, the silicon detector exhibited a complete signal loss, demonstrating its significantly lower radiation tolerance under similar conditions.

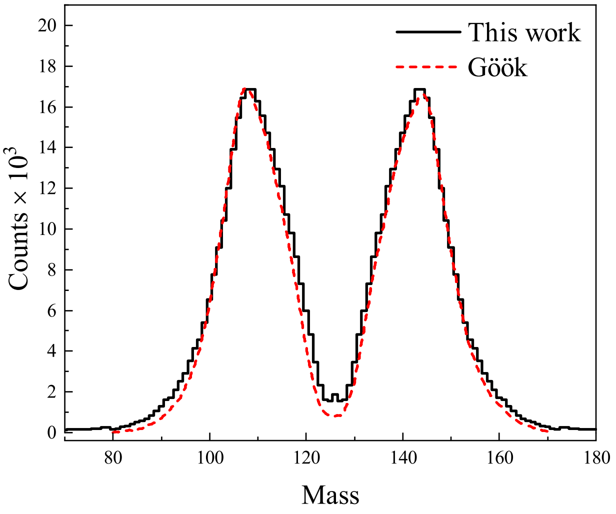

Fig. 9 The mass distribution of fission fragment detected by a solar cell employing Schmitt calibration on the basis of Fig. 7 is depicted in black solid line, while red dashed line represents the mass distribution from [26]. These two distributions are consistent with each other

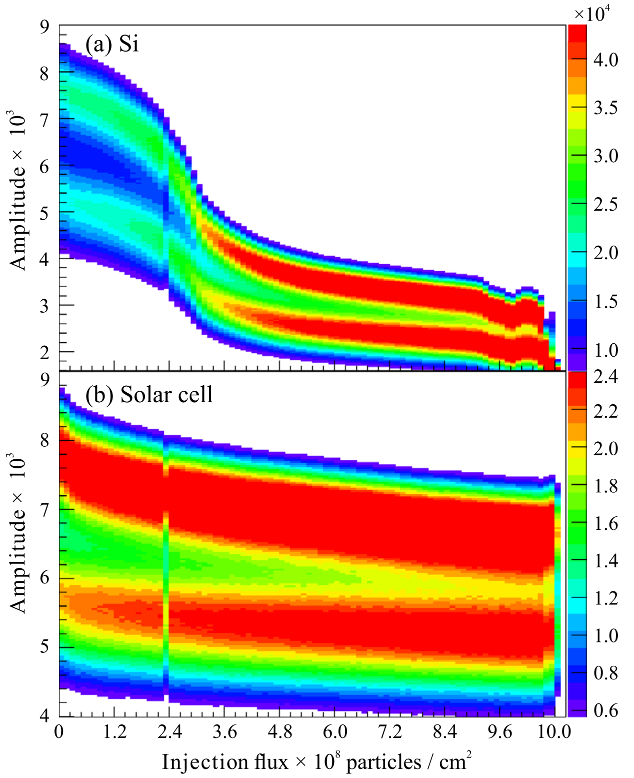

Fig. 10 (Color online)Comparison of pulse-height response as a function of injection flux between a solar cell and a silicon detector of identical size. The matrix in the top panel shows the amplitude distribution with respect to the particle injection flux detected by the silicon detector, whereas the bottom panel displays the corresponding distribution of the solar cell. Each point along the horizontal axis corresponds to a 1-hour integration period of the injection flux. The data point at $x = 2.4$ corresponds to a measurement lasting only 50 min instead of the full hour, resulting in reduced recorded counts and creating the visible gap in the trend

2.4 β detectors: fast plastic scintillators

An auxiliary detector array comprising 36 fast plastic scintillators (11 mm × 11 mm) was integrated into the HALIMA setup for β-particle tagging. Each scintillator, fabricated from EJ-200 plastic scintillator material and 3 mm in thickness, is optically coupled to a Hamamatsu S14160 Multi-Pixel Photon Counter (MPPC) with a sensitive area of 6.4 mm × 6.4 mm. These scintillators and MPPCs were mounted on a PCB, positioned ~ 5 mm downstream from the center of the HALIMA setup. The configuration of β ancillary array is illustrated in Fig. 11. The time resolution of each β detector was measured as 942 ps.

2.5 Electronics and DAQ system

The electronics and data acquisition (DAQ) system of HALIMA is based on the Pixie-16 system developed by XIA LLC, USA. Energy signals from the HPGe detectors,

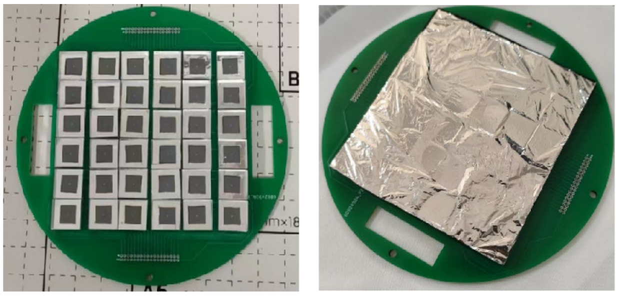
(a) (b)

Fig. 11 (Color online)**a** Scintillator module consisting of thirty-six 11 mm × 11 mm scintillators, each coupled to a 6.4 mm × 6.4 mm MPPC, mounted on a PCB. **b** The assembled scintillator module enclosed with aluminized Mylar film

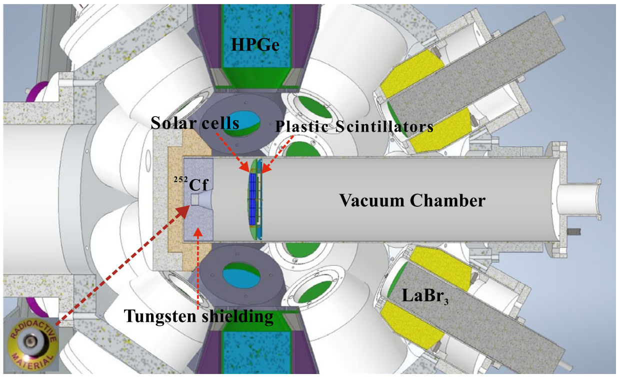

Fig. 12 (Color online)Semi-sectional technical drawing of the HALIMA setup. The inset in the lower-left corner shows the ^{252}Cf source enclosed in tungsten shielding. The arrangement includes HPGe and LaBr$_3$(Ce) detectors, along with the solar cell and plastic scintillator arrays positioned inside the vacuum chamber

BGO and CsI(Tl) anti-Compton shields, and solar cells are digitized by 16 channel, 100 MHz, 14-bit modules, while the energy signals from LaBr$_3$(Ce) detectors and β detectors are digitized by 16 channel, 500 MHz, 14-bit modules, wherein the rise time can be accurately measured. The data were recorded using a general-purpose digital data acquisition system (GDDAQ) [27, 28] and operated in a triggerless mode, which means that all live events are recorded without predefined conditions. This triggerless architecture provides significant flexibility in offline data analysis and event reconstruction [29].

To optimize the fast-timing performance of LaBr$_3$(Ce) detectors, particularly the time resolution and time walk, the waveforms of LaBr$_3$(Ce) detectors are recorded on an event-by-event basis for offline analysis. The waveform recording length was set to 0.2 μs, providing sufficient temporal detail for precise timing studies. The high-voltage supply system is segmented into two parts: Two CAEN N1470 modules are used to power the HPGe detectors, while three ISEG EHS modules are dedicated to supplying the LaBr$_3$(Ce) detectors, CsI(Tl) anti-Compton shields, and BGO detectors.

3 Commissioning with a ^{252}Cf source

A commissioning measurement was performed using a semi-closed ^{252}Cf source with an activity of 100 μCi. The source was encapsulated with a 50 μg/cm^2 Au sputter and mounted on a 0.127 mm thick platinum-clad nickel backing. This configuration ensures that, in each spontaneous fission (SF) event, one fission fragment (FF) recoils into the vacuum chamber, while the complementary FF is absorbed in the backing. Figure 12 illustrates the technical layout of the HALIMA setup in the commissioning phase. The ^{252}Cf source was positioned at the bottom of the vacuum chamber and surrounded by a 40-mm-thick tungsten shield with a cone angle of 18°. This shielding configuration effectively blocks the prompt γ-rays emitted from the source during fission. Following fission, the recoiling FF traverses the 8 cm vacuum gap and is detected by the centrally located solar cell array. In this configuration, the solar cells function as implantation detectors, enabling event-by-event correlation between the FFs and their associated γ-rays. Because the FFs of different masses possess varying velocities, their time-of-flight (TOF) over the 8 cm path introduces a measurable spread, which can be utilized for isomer selection. By gating the signals from the solar cells, isomer-specific events were effectively selected, and the overwhelming background was significantly suppressed. Approximately 4400 h of data acquisition was completed during this commissioning run, yielding approximately $\sim 1.3{\times}10^{11}$ fission events.

In the present work, two complementary approaches were employed to measure the lifetimes of the excited states of interest produced by fission, as illustrated in Fig. 13. The first method, as shown in Fig. 13(a), utilizes the FF-Ge-LaBr$_3$(Ce)-LaBr$_3$(Ce) coincidence technique. In this configuration, a fission event is initially detected by the solar cell array, followed by observation of an isomeric decay involving three or more γ-rays. The excited state of interest, with the lifetime denoted by τ, is fed and decayed via γ_2 and γ_3, which are detected in coincidence by two LaBr$_3$(Ce) detectors. The preceding transition γ_1 is recorded using an HPGe detector. The second approach, as illustrated in Fig. 13(b), involves a β-Ge-LaBr$_3$(Ce)-LaBr$_3$(Ce) coincidence technique based on the fast plastic scintillator array. In this case, γ-rays are emitted following β decay of fission fragments, with the triple γ-ray detection configuration remaining similar to that of the first method.

Prior to the coincidence analysis, the time alignment of all detectors was performed relative to a reference LaBr$_3$(Ce) detector to ensure precise timing. Based on this preliminary data analysis, the FFs selectivity was validated by comparing

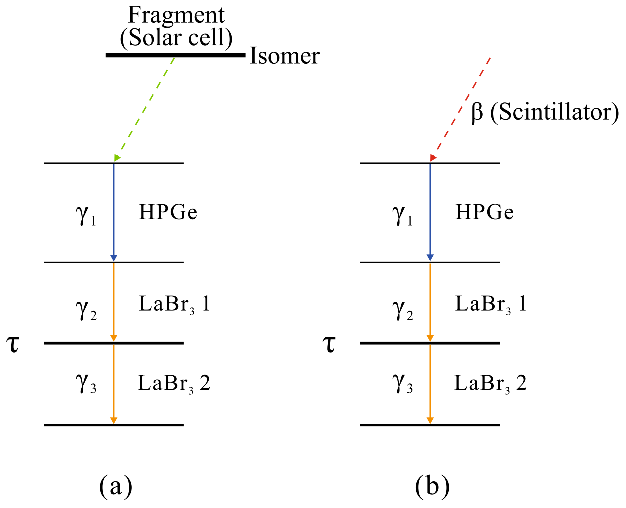

Fig. 13 The principle of two kinds of primary coincidence technique in the present work. **a** Fission fragments-γ_1-γ_2-γ_3 coincidence method: An isomer is implanted into solar cells, followed by isomeric decay with triple or more γ-rays. **b** β-γ_1-γ_2-γ_3 coincidence method: A β decay is measured by fast plastic scintillators, followed by a cascade γ-ray transition. The feeder (γ_2) and decay (γ_3) of excited state of interest represented by τ (orange) are detected by LaBr$_3$(Ce), while the precursor transition (γ_1) is measured by HPGe

γ-ray spectra gated with and without FF detection. This comparison clearly demonstrates the advantage of FF gating in terms of significant background suppression and improved peak-to-background ratio. The lifetimes of the three excited states ranging from a few picoseconds to several hundred nanoseconds were determined by implementing distinct coincidence and lifetime extraction methods. The extracted values showed good agreement with the literature data, confirming the capability of the HALIMA setup to perform precise lifetime measurements over a broad temporal range.

3.1 Time alignment

Owing to variations in electronics, cable lengths, and the use of digitizer cards with different sampling frequencies and bit resolutions, each detector type within the HALIMA setup exhibited a unique timing offset. These offsets lead to misalignments in the time distributions of the detectors when referenced to the reference LaBr$_3$(Ce) detector. To correct this, the timing information, including the initial timestamp and the timing information provided by the CFD filter algorithm, is extracted, allowing for the implementation of time alignment for each detector on a run-by-run basis. For each detector, the relative time difference with respect to the reference LaBr$_3$(Ce) detector was determined by performing a Gaussian fit of the time distribution. The centroid of each distribution was then shifted to 0 ns to achieve synchronization. Figure 14 shows the time difference as a function of the detector ID matrices before and after time alignment. Each unit on the horizontal axis represents individual detector IDs with the HPGe detectors, solar cells, LaBr$_3$(Ce) detectors, and fast plastic scintillators represented by IDs 0–7, 8–43, 44–55, 60–67, 56–59, and 68–99, respectively. As illustrated in Fig. 14(a), the centroids of the time distributions are scattered owing to inherent offsets. After applying the alignment procedure, all the time distributions were successfully centered at approximately 0 ns, as shown in Fig. 14(b), indicating a uniform timing response across all detectors in the array.

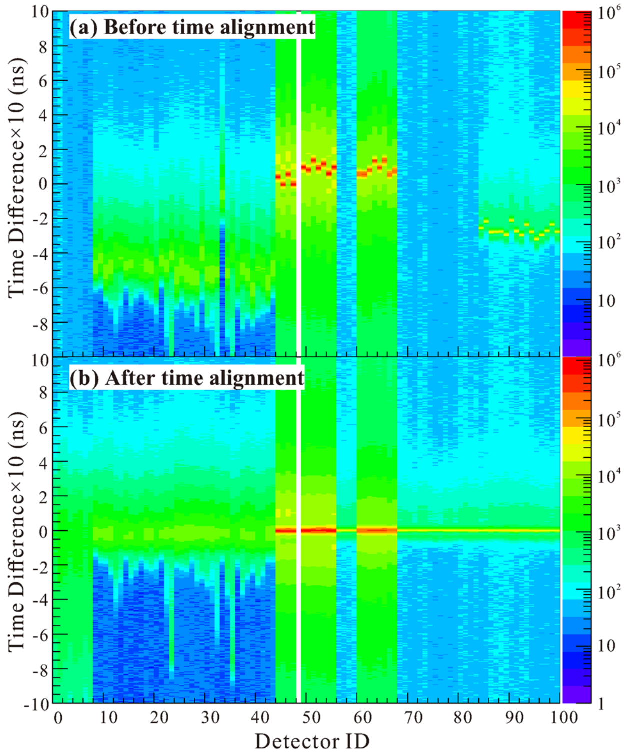

Fig. 14 (Color online)Time alignment matrices before (top panel) and after (bottom panel) time correction. The horizontal axis denotes the detector ID number, whereas the vertical axis shows the time difference between each detector and the reference LaBr$_3$(Ce) detector. Detector IDs 0–7 correspond to HPGe detectors; IDs 8–43 to solar cells; IDs 44–55 and 60–67 to LaBr$_3$(Ce) detectors, and IDs 56–59 and 68–100 to fast plastic scintillators. For detectors with ID = 68–82, the peaks before time alignment are located at 200–300 ns and are not visible here due to the vertical axis being limited to ± 100 ns for clearer visualization of the alignment effect

3.2 Validation of FFs selectivity

The γ-ray spectrum originating from the spontaneous fission of ^{252}Cf is notably complex owing to the presence of emission lines from hundreds of neutron-rich fission fragments. To enhance the selectivity of γ-ray events and suppress the background, the HALIMA setup utilizes a solar cell array to detect fission fragments (FFs), which are then used as triggers for implementing FF-γ coincidence measurements. To evaluate the improvement in selectivity, HPGe-HPGe coincidence spectra were generated under different gating conditions and compared, as shown in Fig. 15. Figure 15(a) shows the HPGe coincidence spectrum of Ge-Ge double events, which were generated using a Ge gate on the 314 keV transition. The γ-rays originating from both the isomeric decay and β decay are shown in the spectrum. In contrast, Fig. 15(b) shows the coincidence spectrum obtained by applying an additional gate on the solar cells, thereby selecting events correlated with fission fragments. Under these conditions, the isomeric state ($19/2^-$, 10 ns) in ^{137}Xe was selectively tagged, and its subsequent γ-ray transitions were prominently visible. As a result, unwanted γ-rays from β decay processes are effectively suppressed, yielding a significantly cleaner spectrum dominated by the 400 keV and 1220 keV transitions.

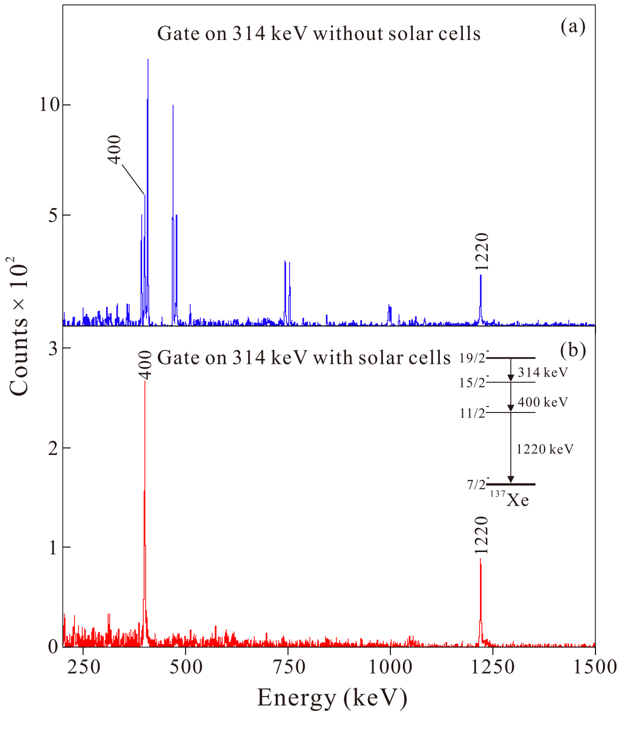

Fig. 15 Energy projection spectra of HPGe detectors using (top) HPGe-HPGe and (bottom) HPGe-HPGe-solar coincidence techniques. The application of an additional gate on solar cells in the bottom panel effectively suppresses contaminant γ-rays, resulting in a cleaner spectrum

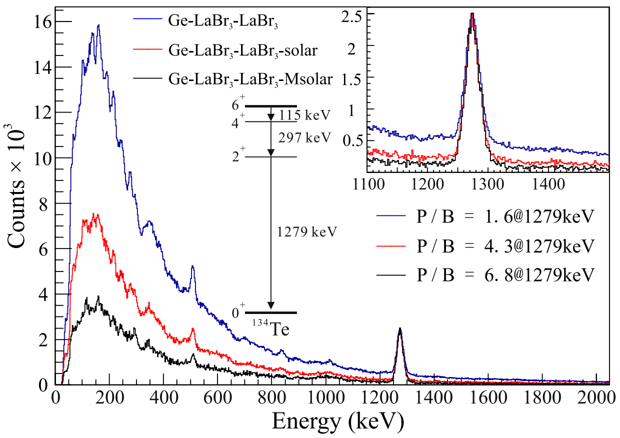

Fig. 16 The energy projection spectra of LaBr$_3$(Ce) demonstrated in three different coincidence methods: (1) Ge-LaBr$_3$(Ce)-LaBr$_3$(Ce) (blue); (2) Ge-LaBr$_3$(Ce)-LaBr$_3$(Ce)-solar (red); and (3) Ge-LaBr$_3$(Ce)-LaBr$_3$(Ce)-Msolar (black), where Msolar denotes a gate on specific mass of FFs. The 1279 keV is shown in the inset. The peak-to-background ratio of 1279 keV was measured under these conditions. With gating on specific mass of ^{134}Te, the peak-to-background ratio of 1279 keV is increased by more than a factor of 4

Beyond its role in enhancing isomer selectivity, gating on FFs offers a significant advantage in suppressing the Compton background, which is particularly critical in fast-timing measurements using LaBr$_3$(Ce)-LaBr$_3$(Ce) coincidences. In such measurements, the background beneath the full-energy peaks can introduce considerable uncertainties, thereby diminishing the precision of lifetime extraction. Furthermore, scattered γ-rays originating primarily from neutron-induced inelastic scattering and Compton scattering of prompt γ-rays within the surrounding components of the HALIMA setup substantially contribute to the background in the LaBr$_3$(Ce) spectra. By utilizing the FF selectivity, this intense background is reduced, thereby improving the peak-to-background ratio. To quantify the performance of this selectivity, a comparative analysis was conducted for the nucleus ^{134}Te, and LaBr$_3$(Ce)-LaBr$_3$(Ce) coincidence spectra were obtained under different gating conditions. In Fig. 16, the LaBr$_3$(Ce) coincidence spectrum was obtained by using a double gate on both 115 and 297 keV, respectively, for Ge and LaBr$_3$(Ce). The peak-to-background ratio obtained for the energy width corresponding to the full width at half maximum of 1279 keV was measured to be 1.6, as shown in the inset of Fig. 16. Upon applying an additional gate on the solar cell signals (gating on FFs), a noticeable reduction in the background, particularly below 600 keV, was observed. Under this condition, the P/B ratio for the 1279 keV peak increased substantially to 4.3. The third case is the LaBr$_3$(Ce) coincidence spectrum employing an additional gate on a specific mass of ^{134}Te. Compared to the Ge-LaBr$_3$(Ce)-LaBr$_3$(Ce) coincidence events, the background in the LaBr$_3$(Ce) spectrum was further suppressed, resulting in a more than fourfold improvement in the P/B ratio.

It should be emphasized that the ^{252}Cf source employed in the present work is a semi-closed source, disabling the employment of the 2E method for determining the masses of FFs detected by solar cells. Therefore, an alternative approach known as the M-V method [30] was exploited, where M and V are the mass and velocity of the FFs, respectively. This method is based on the conservation laws of mass and momentum. Combing Eq. 2 and the following formulas:

$$E = \frac{1}{2}MV^2, \tag{3}$$

$$V = V(M). \tag{4}$$

The velocity distribution as a function of mass was determined using an open ^{252}Cf source developed by the self-transfer technique [31]. The post-neutron mass distribution can then be obtained using an iterative process. Using this method, a mass resolution of approximately 7 atomic mass units (u) (FWHM) was achieved.

3.3 Preliminary results

This subsection presents the lifetime measurements of the three nuclear excited states, ranging from a few picoseconds to several hundred nanoseconds. Specifically, the lifetimes of the two isomers in ^{134}Te and ^{138}Ba were measured using FFs-Ge-Ge/FFs-LaBr$_3$(Ce)-LaBr$_3$(Ce) and β-Ge-LaBr$_3$(Ce)-LaBr$_3$(Ce) coincidence techniques. Additionally, the lifetime of an excited state in ^{132}Te was extracted using the Generalized Centroid Difference (GCD) method based on FFs-Ge-LaBr$_3$(Ce)-LaBr$_3$(Ce) coincidences. The measured lifetimes were in good agreement with previously reported values, validating the reliability of the experimental techniques and analysis methods employed in the present work.

In the case of ^{134}Te, the 6^+ state was identified as a relatively long-lived isomer [32]. As illustrated in Fig. 17, the FFs-Ge-Ge and FFs-LaBr$_3$(Ce)-LaBr$_3$(Ce) coincidence techniques were employed to measure its lifetime. The time difference spectra of both HPGe and LaBr$_3$(Ce) were obtained using a Ge/LaBr$_3$(Ce) gate for both 115 and 297 keV transitions. The coincidence time windows between two γ-rays were set to ± 200 ns for Ge-Ge and ± 4 ns for LaBr$_3$(Ce)-LaBr$_3$(Ce), respectively. Using the slope method, the extracted lifetimes were determined to be 164.04(95) ns from the FFs-Ge-Ge data and 164.7(7) ns from the FFs-LaBr$_3$(Ce)-LaBr$_3$(Ce) data. Both values are in excellent agreement with the previously reported value of 164.1(9) ns [32].

The primary objective of the present work was to measure the sub-nanosecond lifetimes of the nuclear excited states. In the case of ^{138}Ba, the 4^+ state was identified as a short-lived isomer [33], and its lifetime was determined using the β-Ge-LaBr$_3$(Ce)-LaBr$_3$(Ce) coincidence technique. The coincidence time window for detecting the feeder (547 keV) and decay (463 keV) γ-ray transitions with LaBr$_3$(Ce) detectors was set to ± 4 ns, whereas the third γ-ray detected by HPGe was gated on the 1436 keV transition. The coincidence time windows between β- and triple γ-rays were determined based on the correlated prompt time difference distribution. The γ-γ coincidence matrix from LaBr$_3$(Ce) is shown in the top panel of Fig. 18. This matrix clearly reveals 463 keV and 547 keV transition, confirming the correlated decay pathway of the 4^+ state in ^{138}Ba. The time difference spectrum was obtained using an LaBr$_3$(Ce) gate at 463 keV and another LaBr$_3$(Ce) gate at 547 keV, as illustrated in the bottom panel of Fig. 18. A convolution function consisting of Gaussian and exponential distributions was used to fit the time distribution. The extracted half-life of the 4^+ state in ^{138}Ba was found to be 2.02(9) ns, which is in good agreement with the previously reported value of 2.08(6) ns [33].

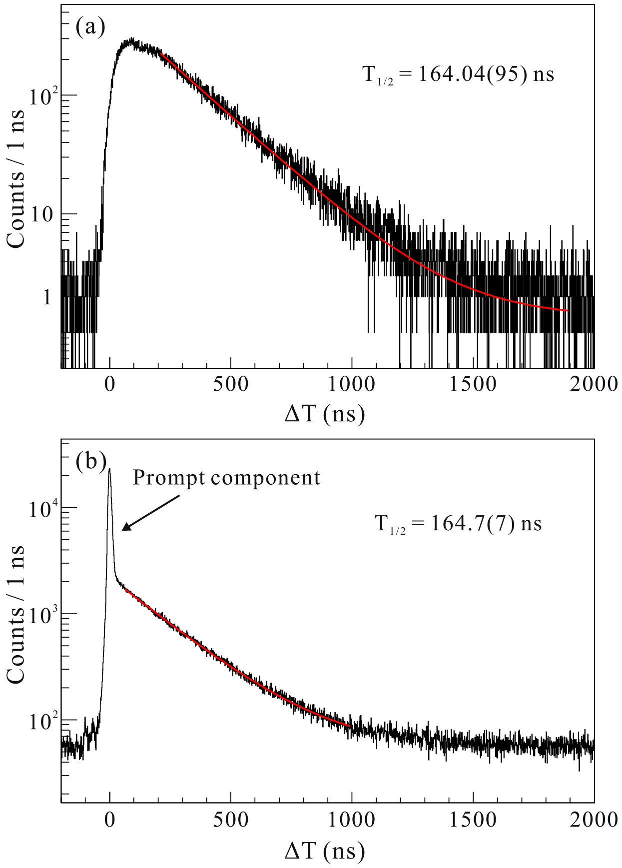

Fig. 17 Delayed coincidence time difference spectra of 6^+ state in ^{134}Te obtained using FFs-γ-γ coincidence method: **a** FFs-HPGe-HPGe and **b** FFs-LaBr$_3$(Ce)-LaBr$_3$(Ce). The half-lives were extracted by exponential fitting to the slope and determined to be 164.04(95) ns and 164.7(7) ns, respectively

The Generalized Centroid Difference (GCD) method provides a more suitable approach for excited states with lifetimes shorter than the intrinsic time resolution of LaBr$_3$(Ce) detectors. The lifetime of the 2_1^+ state of ^{132}Te was determined to be 5(3) ps by implementing γ-γ fast-timing methods based on a mass separator [34]. In the present study, this short-lived excited state was measured using the M(FFs)-γ-γ-γ coincidence technique, where M(FFs)

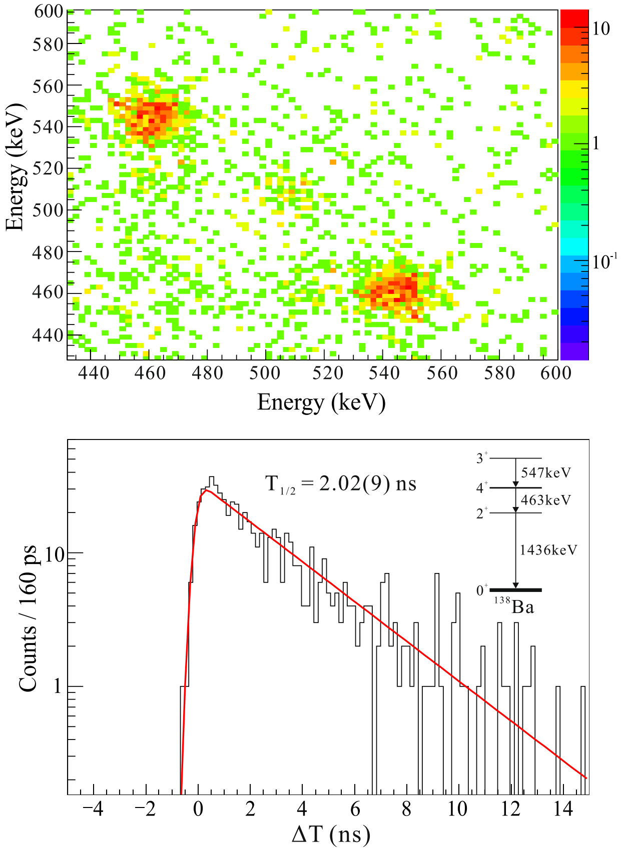

Fig. 18 (Color online)Top panel: γ-γ coincidence matrix of $LaBr_3$(Ce) detectors obtained using the β-HPGe-$LaBr_3$(Ce)-$LaBr_3$(Ce) coincidence technique. Bottom panel: time difference spectrum for the 4^+ state of ^{138}Ba. The half-life was determined to be 2.02(9) ns using convolution method

refers to gating on the known mass of ^{132}Te. The top panel of Fig. 19 presents the γ-γ coincidence matrix of $LaBr_3$(Ce) after background subtraction using HPGe gates on the 103 keV and 151 keV transitions and background gates on either side of the peaks. A strong correlation was observed between the 974 keV and 697 keV transitions. In the GCD method, the centroid difference between the delayed and anti-delayed time distributions is measured. The delayed and anti-delayed time difference spectra for 2_1^+ state of ^{132}Te are presented in the bottom panel of Fig. 19. The time distribution in blue line is "Delayed," corresponds to the start detector is gated on 697 keV (feeder) and the stop detector is gated on 974 keV (decay). Conversely, the red line represents the "Anti-delayed" distribution with the stop detector gated at 697 keV (feeder) and the start detector gated at 974 keV (decay). The background-corrected centroid difference between "Delayed" and "Anti-delayed" was measured to be −769(12) ps. The lifetime was calculated using the following formula:

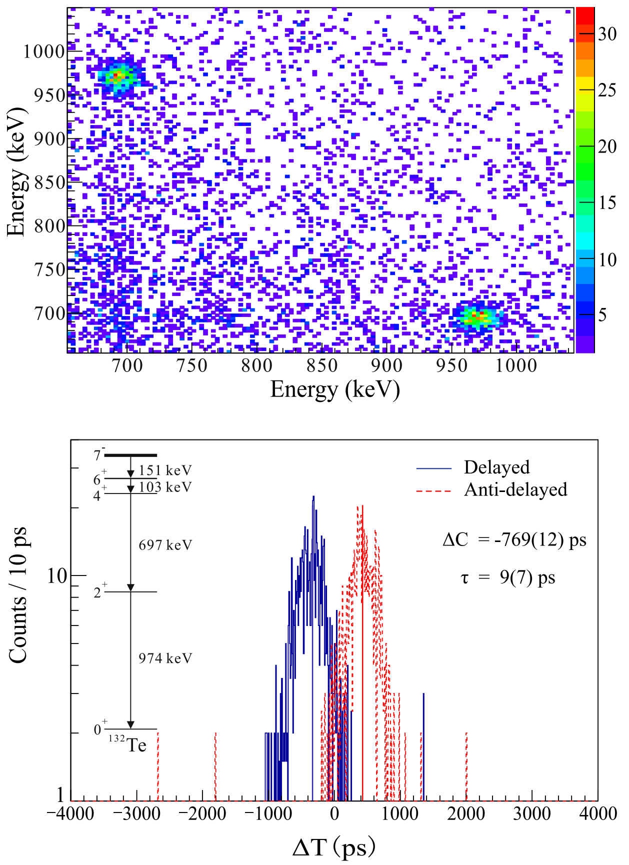

Fig. 19 (Color online)The γ-γ coincidence matrix of $LaBr_3$(Ce) obtained using M(FFs)-γ-γ-γ coincidence technique shown in the top panel. The bottom panel shows the time difference distributions for the delayed and anti-delayed of 2_1^+ states of the ^{132}Te. The mean lifetime was determined to be 9(7) ps using the Generalized Centroid Difference (GCD) method, consistent with the literature value of 5(3) ps [34]

$$2\tau = \Delta C - \mathrm{PRD}. \tag{5}$$

The lifetime was determined to be 9(7) ps, which is in agreement with the values of 5(3) ps in Ref. [34] and 2.15^{+25}_{-20} ps in Ref. [35]. Although the uncertainty in the present measurement is somewhat larger, this is likely attributable to the absence of precise positional calibration among the 36 solar cells used for fission fragment detection. Minor spatial misalignments between the solar cells and the ^{252}Cf source may have introduced additional timing uncertainties, thus affecting the precision of centroid determination. Nonetheless, the close agreement with earlier results validates the reliability of the HALIMA setup and demonstrates its capability to perform accurate sub-nanosecond lifetime measurements in complex fission environments.

4 Summary

A novel hybrid detection system, named HALIMA, was developed and installed at the Institute of Modern Physics to facilitate the measurement of the sub-nanosecond lifetimes of neutron-rich nuclei produced via fission. This system is composed of eight BGO-shielded HPGe detectors and 20 fast $LaBr_3$(Ce) detectors, each shielded with CsI(Tl), offering high-resolution γ-ray energy and timing capabilities. To enhance event selectivity, two specialized ancillary detector arrays were incorporated: a solar cell detector array for detecting fission fragments (FFs) and a fast plastic scintillator array for β-particle detection. These additions enable advanced coincidence techniques, such as FFs/β-Ge-$LaBr_3$ (Ce)-$LaBr_3$(Ce), significantly improving the spectral quality and peak-to-background, thereby allowing precise lifetime measurements. In particular, the implementation of FF gating proved critical in isolating γ-ray cascades of interest by effectively suppressing background contributions from unrelated fission products and β decays. This additional selectivity not only reduced the intense background but also improved the peak-to-background ratio by more than a factor of four, thereby increasing the accuracy of the lifetime measurements. A comprehensive overview of HALIMAs components has been provided, detailing the energy and timing performance of the detectors, the data acquisition (DAQ) system, and the associated electronics architecture.

A commissioning experiment using a ^{252}Cf source was conducted to validate the performance of the HALIMA setup. By applying combined gating to FFs and fast plastic scintillators, the lifetimes of three excited nuclear states in ^{134}Te, ^{138}Ba, and ^{132}Te were measured, covering a range from a few picoseconds to several hundred nanoseconds. The results were in good agreement with the literature values, demonstrating the capability and precision of the HALIMA setup. Furthermore, several excited states with previously unmeasured lifetimes produced by ^{252}Cf fission were identified for the first time, thereby opening new avenues for nuclear structure studies of neutron-rich nuclei.

Looking ahead, the HALIMA system will be used not only to measure the lifetimes of excited states following isomeric or β decay, but also for the lifetimes of prompt γ -rays directly emitted by the FFs of ^{252}Cf, and the source will be placed at the center of the HALIMA array without shielding. To enhance the mass resolution of fission fragments, new ancillary detectors based on Silicon Carbide (SiC) are being developed as next-generation fission detectors. With its advanced detection capabilities, HALIMA will significantly contribute to the systematic study of neutron-rich nuclei produced via neutron-induced fission, extending our understanding of nuclear structures in regions far from stability.

Author contributions All authors contributed to the study conception and design. Material preparation, data collection, and analysis were performed by Zi-Hao Jia, Zhi-Xuan Wang, Jun-Hong Xu, Jian-Hong Li, Wen Liang, Yu-Hong Tan, Wen-Jun Pan, Yu-Xuan Ren, Hai-Xia Li, Rong-Hua Li, Xiu-Hua Wang, and Cui-Hong Chen. The detectors and electronic modules were provided by Yong-De Fang, Wei Wang, Wei Hua, Hong-Yi Wu, Guang-Xin Zhang, Song Guo, Guang-Shun Li, Yun-Hua Qiang, Min-Liang Liu, Bing Ding, Ming-Hui Huang, Ning-Tao Zhang, Bing-Shui Gao, Peng Ma, He-Run Yang, Ruo-Fu Chen, Hai-Bo Yang, Jian-Song Wang, Xiao-Hui Sun, Zhi-Huan Li, and Hui Hua. The fund was supported by Si-Cheng Wang, Cen-Xi Yuan, Xin-Xing Xu, Xiao-Hong Zhou, Zai-Guo Gan, and Yu-Hu Zhang. The first draft of the manuscript was written by Zi-Hao Jia. The manuscript was revised by Yong-De Fang and M. Kumar Raju. All authors commented on the previous versions of the manuscript. All authors read and approved the final manuscript.

Data availability The data that support the findings of this study are openly available in Science Data Bank at https://cstr.cn/31253.11.sciencedb.j00186.00749 and https://www.doi.org/10.57760/sciencedb.j00186.00749.

Declarations

Conflict of interest The authors declare that they have no conflict of interest.

References

1. J.-M. Régis, L.M. Fraile, M. Rudigier, γ-γ fast timing with high-performance $LaBr_3$(Ce) scintillators. Prog. Part. Nucl. Phys. **141**, 104152 (2025). https://doi.org/10.1016/j.ppnp.2024.104152
2. M. Rudigier, Zs. Podolyák, P. H. Regan et al., FATIMA — fast timing array for DESPEC at FAIR. Nucl. Instrum. Meth. Phys. Res. Sect. A **969**, 163967 (2020). https://doi.org/10.1016/j.nima.2020.163967
3. B. Moon, J. Lee, Y. Jang et al., New fast-timing γ-ray detection system in Korea: KHALA. Nucl. Instrum. Meth. Phys. Res. Sect. B **541**, 253–256 (2023). https://doi.org/10.1016/j.nimb.2023.05.035
4. V. Piau, A. Göök, S. Oberstedt et al., Characterization of isomers produced by the spontaneous fission of ^{252}Cf with the vespa setup. Euro. Phys. J. A **61**, 5 (2025). https://doi.org/10.1140/epja/s10050-024-01470-9
5. J.-M. Régis, G.S. Simpson, A. Blanc et al., Germanium-gated γ–γ fast timing of excited states in fission fragments using the EXILL & FATIMA spectrometer. Nucl. Instrum. Meth. Phys. Res. Sect. A **763**, 210–220 (2014). https://doi.org/10.1016/j.nima.2014.06.004
6. M. Lebois, N. Jovancevic, D. Thisse et al., The ν-ball γ-spectrometer. Nucl. Instrum. Meth. Phys. Res. Sect. A **960**, 163580 (2020). https://doi.org/10.1016/j.nima.2020.163580
7. E.R. Gamba, A.M. Bruce, M. Rudigier et al., Treatment of background in γ- γ fast-timing measurements. Nucl. Instrum. Meth. Phys. Res. Sect. A **928**, 93–103 (2019). https://doi.org/10.1016/j.nima.2019.03.028
8. F. Kandzia, G. Belier, C. Michelagnoli et al., Development of a liquid scintillator based active fission target for FIPPS. Europ. Phys. J. A **56**, 207 (2020). https://doi.org/10.1140/epja/s10050-020-00201-0
9. G.S. Simpson, W. Urban, K. Sieja et al., Near-yrast, medium-spin, excited states of ^{91} Rb, ^{93} Rb, and ^{95} Rb. Phys. Rev. C **82**, 024302 (2010). https://doi.org/10.1103/PhysRevC.82.024302

10. D.C. Radford, ESCL8R and LEVIT8R: Software for interactive graphical analysis of HPGe coincidence data sets. Nucl. Instrum. Meth. Phys. Res. Sect. A **361**, 297–305 (1995). https://doi.org/10.1016/0168-9002(95)00183-2
11. R. Britton, J.L. Burnett, A.V. Davies et al., Improving the effectiveness of a low-energy Compton suppression system. Nucl. Instrum. Meth. Phys. Res. Sect. A **729**, 64–68 (2013). https://doi.org/10.1016/j.nima.2013.06.111
12. S. Aogaki, D.L. Balabanski, R. Borcea et al., A setup for high-energy γ-ray spectroscopy with the ELI-NP large-volume $LaBr_3$: Ce and $CeBr_3$ detectors at the 9 MV Tandem accelerator at IFIN-HH. Nucl. Instrum. Meth. Phys. Res. Sect. A **1056**, 168628 (2023). https://doi.org/10.1016/j.nima.2023.168628
13. M. Gierlik, S. Borsuk, Z. Guzik et al., Application of the anti-compton detector in neutron activation analysis techniques. Nucl. Instrum. Meth. Phys. Res. Sect. A **788**, 54–58 (2015). https://doi.org/10.1016/j.nima.2015.03.051
14. W.K. Warburton, W. Hennig, New algorithms for improved digital pulse arrival timing with sub-GSPS ADCS. IEEE Trans. Nucl. Sci. **64**, 2938–2950 (2017). https://doi.org/10.1109/TNS.2017.2766074
15. J.-M. Régis, H. Mach, G.S. Simpson et al., The generalized centroid difference method for picosecond sensitive determination of lifetimes of nuclear excited states using large fast-timing arrays. Nucl. Instrum. Meth. Phys. Res. Sect. A **726**, 191–202 (2013). https://doi.org/10.1016/j.nima.2013.05.126
16. G. Siegert, Photovoltaic cells as fission product detectors. Nucl. Instrum. Meth. **164**, 437–438 (1979). https://doi.org/10.1016/0029-554X(79)90076-4
17. N.N. Ajitanand, R.P. Anand, S.R.S. Murthy et al., The photovoltaic cell—an eminent fission fragment detector. Nucl. Instrum. Meth. Phys. Res. Sect. A **300**, 354–356 (1991). https://doi.org/10.1016/0168-9002(91)90448-Y
18. A.G. Smith, R.M. Wall, D. Patel et al., Lifetimes of yrast rotational states of the fission fragments ^{100}Zr and ^{104}Mo measured using a differential plunger. J. Phys. G: Nucl. Part. Phys. **28**, 2307 (2002). https://doi.org/10.1088/0954-3899/28/8/316
19. C. Gautherin, M. Houry, W. Korten et al., New isomeric states in ^{152}Nd, ^{154}Nd, ^{156}Nd produced by spontaneous fission of Cf-252. Europ. Phys. J. A **1**, 391–397 (1998). https://doi.org/10.1007/s100500050074
20. R. Pérez Sánchez, B. Jurado, P. Marini et al., Experimental set-up for the simultaneous measurement of fission and γ-emission probabilities induced by transfer or inelastic-scattering reactions. Nucl. Instrum. Meth. Phys. Res. Sect. A **933**, 63–70 (2019). https://doi.org/10.1016/j.nima.2019.04.084
21. J.D. Koglin, J.T. Harke, S.E. Fisher et al., DEATH-STAR: silicon and photovoltaic fission fragment detector arrays for light-ion induced fission correlation studies. Nucl. Instrum. Meth. Phys. Res. Sect. A **854**, 64–69 (2017). https://doi.org/10.1016/j.nima.2017.02.054
22. S. Boorboor, S.A.H. Feghhi, H. Jafari, Funneling effect of alpha particles on the charge collection efficiency in N type silicon surface barrier detector. Nucl. Instrum. Meth. Phys. Res. Sect. B **325**, 1–4 (2014). https://doi.org/10.1016/j.nimb.2014.01.020
23. C. Budtz-Jørgensen, H.-H. Knitter, Ch. Straede et al., A twin ionization chamber for fission fragment detection. Nucl. Instrum. Meth. Phys. Res. Sect. A **258**, 209–220 (1987). https://doi.org/10.1016/0168-9002(87)90058-1
24. H.W. Schmitt, W.E. Kiker, C.W. Williams, Precision measurements of correlated energies and velocities of ^{252} Cf fission fragments. Phys. Rev. **137**, B837–B847 (1965). https://doi.org/10.1103/PhysRev.137.B837
25. E. Weissenberger, P. Geltenbort, A. Oed et al., Energy calibration of surface barrier detectors for fission fragments. Nucl. Instrum. Meth. Phys. Res. Sect. A **248**, 506–515 (1986). https://doi.org/10.1016/0168-9002(86)91041-7
26. A. Göök, F.-J. Hambsch, M. Vidali, Prompt neutron multiplicity in correlation with fragments from spontaneous fission of ^{252} Cf. Phys. Rev. C **90**, 064611 (2014). https://doi.org/10.1103/PhysRevC.90.064611
27. H.Y. Wu, Z.H. Li, H. Tan et al., A general-purpose digital data acquisition system (GDDAQ) at Peking University. Nucl. Instrum. Meth. Phys. Res. Sect. A **975**, 164200 (2020). https://doi.org/10.1016/j.nima.2020.164200
28. D.W. Luo, H.Y. Wu, Z.H. Li et al., Performance of digital data acquisition system in gamma-ray spectroscopy. Nucl. Sci. Tech. **32**, 79 (2021). https://doi.org/10.1007/s41365-021-00917-8
29. S. Das, S. Samanta, R. Banik et al., A Compton suppressed detector multiplicity trigger based digital DAQ for gamma-ray spectroscopy. Nucl. Instrum. Meth. Phys. Res. Sect. A **893**, 138–145 (2018). https://doi.org/10.1016/j.nima.2018.03.035
30. S.L. Whetstone, Coincident time-of-flight measurements of the velocities of ^{252}Cf fission fragments. Phys. Rev. **131**, 1232–1243 (1963). https://doi.org/10.1103/PhysRev.131.1232
31. H.L. Adair, P.R. Kuehn, Preparation of ^{252}Cf neutron and fission-fragment sources. Nucl. Instrum. Meth. **114**, 327–332 (1974). https://doi.org/10.1016/0029-554X(74)90551-5
32. G. Häfner, R. Lozeva, H. Naïdja et al., First lifetime investigations of $N > 82$ iodine isotopes: the quest for collectivity. Phys. Rev. C **104**, 014316 (2021). https://doi.org/10.1103/PhysRevC.104.014316
33. B. Roussière, M.A. Cardona, I. Deloncle et al., Half-life measurements of ^{137,139}Cs excited nuclear states. Europ. Phys. J. A **47**, 106 (2011). https://doi.org/10.1140/epja/i2011-11106-4
34. D. Kumar, T. Bhattacharjee, S.S. Alam et al., Lifetimes and transition probabilities for low-lying yrast levels in ^{130,132}Te. Phys. Rev. C **106**, 034306 (2022). https://doi.org/10.1103/PhysRevC.106.034306
35. M. Danchev, G. Rainovski, N. Pietralla et al., One-phonon isovector $2^+_{1,\mathrm{MS}}$ state in the neutron-rich nucleus ^{132}Te. Phys. Rev. C **84**, 061306 (2011). https://doi.org/10.1103/PhysRevC.84.061306

Authors and Affiliations

Zi-Hao Jia[1,2] · Yong-De Fang[1,2] · Si-Cheng Wang[1,2] · Wei Hua[3,4] · Hong-Yi Wu[5,6] · Guang-Xin Zhang[3] · Cen-Xi Yuan[3] · Zhi-Xuan Wang[3] · Jun-Hong Xu[1,2] · Jian-Hong Li[1,2] · Wen Liang[1,2] · Yu-Hong Tan[1,2] · Wen-Jun Pan[6] · Yu-Xuan Ren[6] · M. Kumar Raju[7] · Song Guo[1,2] · Guang-Shun Li[1,2] · Yun-Hua Qiang[1,2] · Min-Liang Liu[1,2] · Bing Ding[1,2] · Ming-Hui Huang[1,2] · Ning-Tao Zhang[1,2] · Bing-Shui Gao[1,2] · Peng Ma[1,2] · He-Run Yang[1,2] · Ruo-Fu Chen[1,2] · Hai-Xia Li[1,2] · Rong-Hua Li[1,2] · Xiu-Hua Wang[1,2] · Cui-Hong Chen[1,2] · Hai-Bo Yang[1,2] · Jian-Song Wang[8] · Xiao-Hui Sun[8] · Zhi-Huan Li[6] · Hui Hua[6] · Wei Wang[3] · Xin-Xing Xu[1,2] · Xiao-Hong Zhou[1,2] · Zai-Guo Gan[1,2] · Yu-Hu Zhang[1,2]

✉ Yong-De Fang
fangyd@impcas.ac.cn

✉ Si-Cheng Wang
wangsicheng@impcas.ac.cn

✉ Wei Hua
huaw@mail.sysu.edu.cn

✉ Hong-Yi Wu
wuhongyi@pku.edu.cn

[1] State Key Laboratory of Heavy Ion Science and Technology, Institute of Modern Physics, Chinese Academy of Sciences, Lanzhou 730000, China

[2] School of Nuclear Science and Technology, University of Chinese Academy of Science, Beijing 100049, China

[3] Sino-French Institute of Nuclear Engineering and Technology, Sun Yat-Sen University, Zhuhai 519082, China

[4] Guangxi Key Laboratory of Nuclear Physics and Nuclear Technology, Guangxi Normal University, Guilin 541004, China

[5] Key Laboratory of Nuclear Data, China Institute of Atomic Energy, Beijing 102413, China

[6] School of Physics and State Key Laboratory of Nuclear Physics and Technology, Peking University, Beijing 100871, China

[7] Department of Physics, GITAM School of Science, GITAM University, Visakhapatnam 530045, India

[8] School of Science, Huzhou University, Huzhou 313000, China